TU Delft

Delft University of Technology

An experimentally validated analytical model for natural electrolyte recirculation in an alkaline water electrolyser

Deiters, G. B.; de Vries, J. R.; Haverkort, J. W.

DOI
10.1016/j.ijhydene.2025.152053

Publication date
2025

Document Version
Final published version

Published in
International Journal of Hydrogen Energy

Citation (APA)
Deiters, G. B., de Vries, J. R., & Haverkort, J. W. (2025). An experimentally validated analytical model for natural electrolyte recirculation in an alkaline water electrolyser. *International Journal of Hydrogen Energy*, *188*, Article 152053. https://doi.org/10.1016/j.ijhydene.2025.152053

Important note
To cite this publication, please use the final published version (if applicable).
Please check the document version above.

Copyright
Other than for strictly personal use, it is not permitted to download, forward or distribute the text or part of it, without the consent of the author(s) and/or copyright holder(s), unless the work is under an open content license such as Creative Commons.

Takedown policy
Please contact us and provide details if you believe this document breaches copyrights.
We will remove access to the work immediately and investigate your claim.

This work is downloaded from Delft University of Technology.
For technical reasons the number of authors shown on this cover page is limited to a maximum of 10.

International Journal of Hydrogen Energy 188 (2025) 152053

Contents lists available at ScienceDirect

International Journal of Hydrogen Energy

journal homepage: www.elsevier.com/locate/he

An experimentally validated analytical model for natural electrolyte recirculation in an alkaline water electrolyser

G.B. Deiters *, J.R. de Vries, J.W. Haverkort

Delft University of Technology, Process & Energy Department, Leeghwaterstraat 39, Delft, 2628 CB Delft, The Netherlands

ARTICLE INFO

Keywords:
Alkaline water electrolysis
Air-lift reactor
Natural recirculation

ABSTRACT

The rising gas bubbles that are generated in an electrolyser cause electrolyte to flow upwards. By adding a downcomer after separating the gas, the electrolyte will recirculate through natural convection without a pump. We measured the resulting flow rate as a function of current density and electrode–wall distance in a zero-gap alkaline water electrolysis cell. Next, we developed a simple but surprisingly accurate fully analytical model to describe this flow rate as a function of various geometrical and operational parameters. From this model, we derive fully explicit expressions for the optimal electrode–wall distance. For our setup of 0.4 m height we find that values of 1.5–1.9 mm maximise mass transfer, velocity, or minimise the ohmic drop. The electrolyte flow rate is maximised for larger distances, around 6 mm. The accuracy, simplicity, and generality of our analytical model will be useful for the design and optimisation of a variety of gas-evolving electrolysers, including lab-scale as well as industrial reactors.

1. Introduction

Most alkaline water electrolysers use a pump to circulate the electrolyte. The pump is used to remove heat from the system, to direct the produced gas bubbles towards the gas–liquid separators, and to recombine anolyte and catholyte streams, negating losses due to diffusion limitations [1,2]. As an alternative to a pump, the buoyancy of the gas can be used to generate a liquid circulation. This eliminates maintenance and operational costs. Here we consider three significant fields of application in the chemical industry: air-lift reactors, chlor-alkali electrolysers and water electrolysers.

Air-lift reactors are the most mature technology of the three. For example, they are used in wastewater treatment, fermentation and the processing of algae. Because of this broad application, several models already exist in the literature. Chisti and Moo-Young [3] provide an extensive overview of the older literature, focusing on multiphase hydrodynamics. Notable examples are the numerical model by Young et al. [4], which was later revised and simplified in Ref. [5], and the CFD model by Mudde and van den Akker [6]. These models have in common that the riser is modelled with friction factors instead of laminar flow because air-lift reactors typically have large channel dimensions. Conversely, the channels in water electrolysers are generally smaller, as the components are often stacked in a thin sandwich-like structure to reduce ohmic losses.

A different application for gas-driven circulation is the chlor-alkali process. Here, sodium hydroxide and chlorine gas are produced in an electrolytic process. It is essential to have good mass transfer near the anodes, which is why the produced chlorine gas is often used to drive electrolyte recirculation. Typically, each cell has its own downcomer by introducing a weir plate [7]. For example, the mercury cell electrolyser design of De Nora S.p.A uses a series of inclined baffles [8,9] called runner anodes, see Fig. 1.

A few smaller alkaline water electrolyser manufacturers use the same air-lift principle to drive electrolyte circulation. These include Hydrogenics (previously Vandenborre) [11,12], Stiesdal Ptx Technologies A/S [13], and Next Hydrogen [14]. A patent by the latter company integrates cooling tubes, as shown in Fig. 2. Besides these conventional electrolysers, other electrolyser designs also use natural recirculation, without using a dedicated downcomer. For example, the lantern-blades [15] or the Venetian blind electrodes [16] make use of natural recirculation on a smaller scale associated with the electrode structure.

In the scientific literature for water electrolysers, Hine and Murakami [17] found a recirculation velocity of about 0.2 m/s at a 1 A/cm^2 current density for an electrode–wall distance of 5–10 mm in their 89-cm tall alkaline water electrolyser with internal downcomer. They found a stark increase in resistivity for electrolyte gaps below 5 mm. Similar velocities were found by Roušar [18] in a 70-cm tall electrolyser with an external downcomer. Roušar has developed a model for this electrolyser using energy balances. The pressure drop was

* Corresponding author.
E-mail addresses: G.B.Deiters@tudelft.nl (G.B. Deiters), J.W.Haverkort@tudelft.nl (J.W. Haverkort).

https://doi.org/10.1016/j.ijhydene.2025.152053
Received 18 July 2025; Received in revised form 18 September 2025; Accepted 14 October 2025
Available online 23 October 2025
0360-3199/© 2025 The Authors. Published by Elsevier Ltd on behalf of Hydrogen Energy Publications LLC. This is an open access article under the CC BY license (http://creativecommons.org/licenses/by/4.0/).

Nomenclature

Symbols

$\dot{\gamma}$	Shear rate (1/s)
ε	Gas fraction (–)
$\mathcal{V}_m$	Molar volume (m^3/mol)
μ	Electrolyte dynamic viscosity (Pa s)
ρ	Electrolyte density (kg/m^3)
F	Faraday's constant (C/mol)
f_i	Inertial correction factor (–)
f_v	Viscous riser correction factor (–)
g	Gravitational acceleration (m/s^2)
h	Electrode height (m)
j	Current Density (A/m^2)
l	Electrode–wall distance (m)
n	Electrons per gas molecule (–)
p	Pressure (Pa)
Q	Flow rate (m^3/s)
Q_i	Inertial characteristic flow rate (m^3/s)
Q_v	Viscous characteristic flow rate (m^3/s)
$Q_{v,D}$	Viscous characteristic flow rate in the downcomer (m^3/s)
W	Superficial velocity (m/s)
w	Velocity (m/s)

Subscripts

∞	$l \to \infty$
$\langle\cdots\rangle$	Average over height $\frac{1}{h}\int_0^h \ldots dz$
y	y-direction
g	Gas
l	Liquid
max	Maximum
S	Slip velocity

measured as a function of flow rate and expressed in an equation. The liquid recirculation flow, and therefore the pumping power, could thus be calculated and balanced to the energy generated by the buoyancy of the produced bubbles.

In a series of German papers [19–22], Wolfgang Thiele and Martin Schleiff from the University of Halle-Wittenberg set out a simple analytical model. Here, they modelled the gas fraction and recirculation velocity for planar electrodes, with gas produced in between. In this model, a laminar Hagen–Poiseuille pressure relation is used, and the gas slip is neglected. Furthermore, they introduced a method for approximately relating the top and average gas fractions. With the gas fraction, the ohmic resistance can be estimated since bubbles are assumed to block the path of ions. Using this, they obtained an approximate expression for the gap width that maximises the energy efficiency. This is typically around 1 mm and scales with the square root of the current density, similar to the experiments of Hine and Murakami [17]. However, it does not allow for explicit analytical solutions and requires the coupled equations to be solved numerically.

Similarly, the work of Gol'dberg [23] presents equations that must be solved numerically for a setup with a small gap between the electrode and the separator. It addresses the lack of hydraulic resistance models used in previous works. This is then implemented and used to determine the optimal gap between the electrodes for minimum electrical resistance.

Recently, Haverkort [24] investigated natural recirculation for a zero-gap design. Here, several explicit analytical expressions were derived, using a single-phase turbulent flow pressure drop relation.

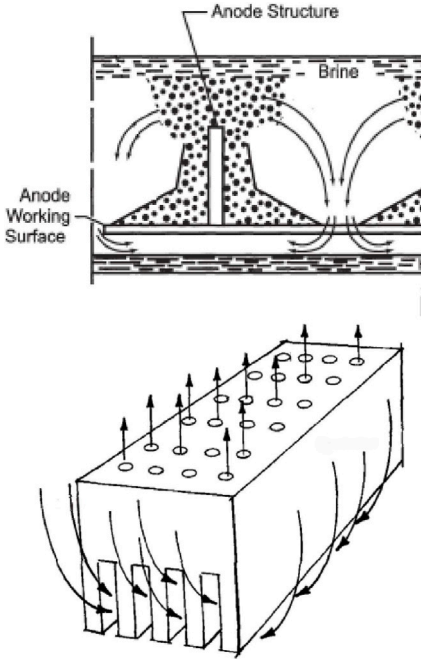

Fig. 1. Simple gas lift recirculation in monopolar mercury chlor-alkali cells. The top figure is a De Nora S.p.A. chlor-alkali mercury cell with inclined 'runner anodes'. The bottom figure shows an anode brine circulation.
Source: Adapted from Ref. [10].

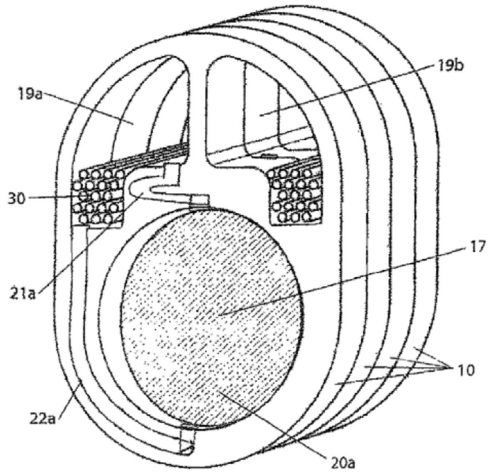

Fig. 2. A stacked electrode design with internal gas–liquid separation (19a, 19b) and integrated heat exchangers (30) by Next Hydrogen taken from Ref. [14]. Here, the electrolyte circulates back into the cell using an external downcomer channel (22a).

Despite these model developments, simple, explicit analytical scaling relations for the flow and gas fraction are lacking. These could greatly improve the understanding of the system and, thus, improve the design process.

This study introduces a model that allows explicit, approximate analytical expressions for the recirculation velocity as a function of electrode–wall distance and current density. At the same time, it is general enough to include both laminar and turbulent friction through empirical parameters with a clear physical meaning that can be measured independently. The model is validated by experimental data from an in-house zero-gap natural recirculation electrolyser.

2. Theory

The electrolyser used in this study can be subdivided into a *riser*, where the gas is produced, and an external *downcomer*, which connects the riser's inlet and outlet with a gas–liquid separator. This division is illustrated in the schematic of Fig. 4.

2.1. The riser

When water is converted into hydrogen and oxygen gas in the riser, this creates a multiphase mixture of gas and liquid. Since the density of the gases is far lower than that of the liquid, this effectively creates a void with a fraction of ε. The overall density of the multiphase flow also reduces with this increasing fraction of gas by a factor of $1-\varepsilon$. Since the downcomer is still filled with water without gas, a weight difference exists, which creates an imbalance in the stationary fluid. The stationary fluid must accelerate to compensate for this imbalance, and it will continue accelerating until it balances with the system's frictional flow forces. The gas injection in one of the riser compartments is illustrated in Fig. 3. This gas volume injected per unit electrode area is given by Faraday's law of electrolysis as $U_g = j\mathcal{V}_m/nF$ [m/s]. The constant $F \approx 96485.3321$ C/mol is Faraday's constant, converting Coulombs to moles of electrons, n is the number of gas molecules produced per electron, $\mathcal{V}_m$ is the molar gas volume, converting these moles gas to cubic meters, and j is the current per unit area, or simply current density. For an ideal gas $\mathcal{V}_m = RT/p$, but at elevated temperatures, we also have to account for the water vapour content of the bubbles. We will assume U_g to be constant over height, which is the case for constant current density and molar volume $\mathcal{V}_m$ across the electrolyser. Conservation of volume gives $U_g h l_y = W_g l l_y$, with W_g the volumetric gas flux in the vertical direction, so

$$W_g = \frac{j\mathcal{V}_m}{nF}\frac{h}{l}. \tag{1}$$

Assuming all gas is stripped in the gas–liquid separator and a pure liquid flow re-enters the riser at the bottom, the average gas fraction over the riser height, h, is given by Eq. (36) in Appendix A in the Supplementary Data. Here, we obtain a result for the average gas fraction in the riser in a similar fashion as Refs. [25–27]

$$\langle\varepsilon\rangle \approx \frac{1}{\frac{1}{\varepsilon_{max}} + \frac{W_l + w_S}{W_g/2}} \tag{2}$$

Thus, the average gas fraction increases linearly with low values of $\frac{W_g}{W_l+w_S}$. At high values of $\frac{W_g}{W_l+w_S}$, the average gas fraction tends to a maximum ε_{max}. This maximum can be taken as the maximum packing fraction of monodisperse spheres, $\varepsilon_{max} = \pi/3\sqrt{2} \approx 0.74$; however, a different value may be more appropriate to describe experiments with electrolytically generated bubbles, where bubble sizes are polydispersed. Experiments of Ref. [28] showed a good fit with $w_S = 0$ and $\varepsilon_{max} = 0.7$. Ref. [29] used gas-sparging and found a fine fit with $w_S = 5$ cm/s and $\varepsilon_{max} = 1$. Some works argue that hindrance should be included so that the slip velocity decreases with increasing gas fraction [30–32]. Dedicated experiments [30] have found values as small as $\varepsilon_{max} = 0.2$, while this value seems to be increasing with increasing electrolyte ionic strength [32]. Recently, significant coalescence of the gas bubbles has been reported for gas fractions between 0.25 and 0.4 in a 1.5-m classical electrolyser without a separator [33] leading to slug flow. Here, we keep w_S and ε_{max} as two free, but constant, parameters whose exact value depends on the electrolyte and electrolyser geometry.

2.2. Pressure balance

As mentioned before, an increased gas fraction in the riser creates a net force, or pressure difference, on the fluid

$$\Delta p_H = \underbrace{\rho g h}_{\text{Downcomer}} - \underbrace{\rho g h(1-\langle\varepsilon\rangle)}_{\text{Riser}} = \rho g h \langle\varepsilon\rangle \tag{3}$$

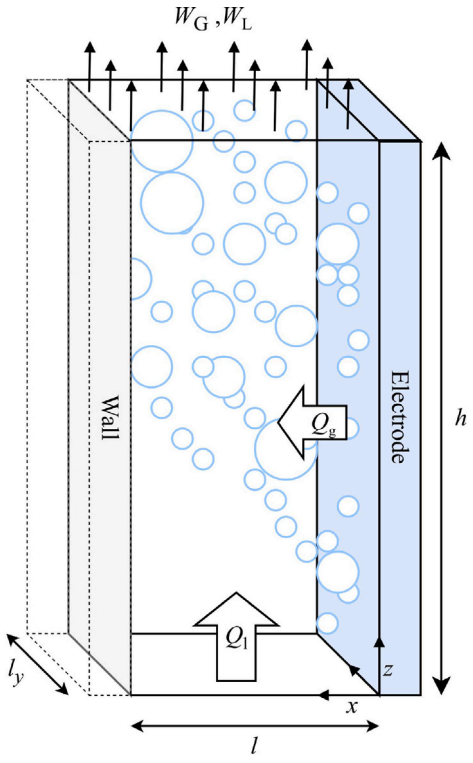

Fig. 3. Schematic of the gas-filled riser. The electrode on the right injects gas with a rate of $Q_g = \frac{j\mathcal{V}_m}{nF} h l_y$, which combines with the recirculated electrolyte flow Q_l to get the exiting multiphase flow at the top with superficial gas and superficial liquid velocities of W_g and W_l, respectively. In this setup, the 'Wall' is the PMMA endplate. In an industrial zero-gap electrolyser stack, this will be the bipolar plate, which distributes the current to the electrode. However, it may also be the membrane in a traditional gap-electrolyser, or the counter-electrode in a membraneless electrolyser. In this last case, the channel will be shared by the cathode and anode sides.

In steady state, this pressure drop balances with the frictional pressure drop in the riser and downcomer: $\Delta p_H = \Delta p_f$. We write the frictional pressure drop in a general form

$$\Delta p_f = \frac{1}{2}\rho g h \left(\frac{Q_l}{Q_v} + \left(\frac{Q_l}{Q_i}\right)^2\right) \tag{4}$$

consisting of a linear and a quadratic term. These terms contain the characteristic flow rates Q_v and Q_i, which describe the pressure losses created by the recirculation flow rate. These two coefficients should be obtained from pressure drop measurements or used as model fitting parameters.

The second, quadratic term is mostly associated with the potential turbulence in the riser and irreversible losses due to, for example, the bends, contractions and expansions in the downcomer ducts.

The first, linear term describes the laminar losses in the riser and downcomer. The coefficient Q_v in equation Eq. (10) can be further divided into a contribution of the downcomer, $Q_{v,D}$, and the riser as

$$Q_v^{-1} = Q_{v,D}^{-1} + \frac{24\mu}{\rho g l^3 l_y} \tag{5}$$

When the flow is laminar, the contribution of the downcomer to this viscous pressure drop, $Q_{v,D}$, can be estimated using the Hagen–Poiseuille equation. In this case, $Q_{v,D}$ is inversely proportional to the length of the downcomer piping. Increasing the diameter will reduce the pressure drop and thus increase $Q_{v,D}$. For many industrial systems, a single downcomer will combine the flows of the different cells. In this case, the flow will most likely be turbulent, meaning that the

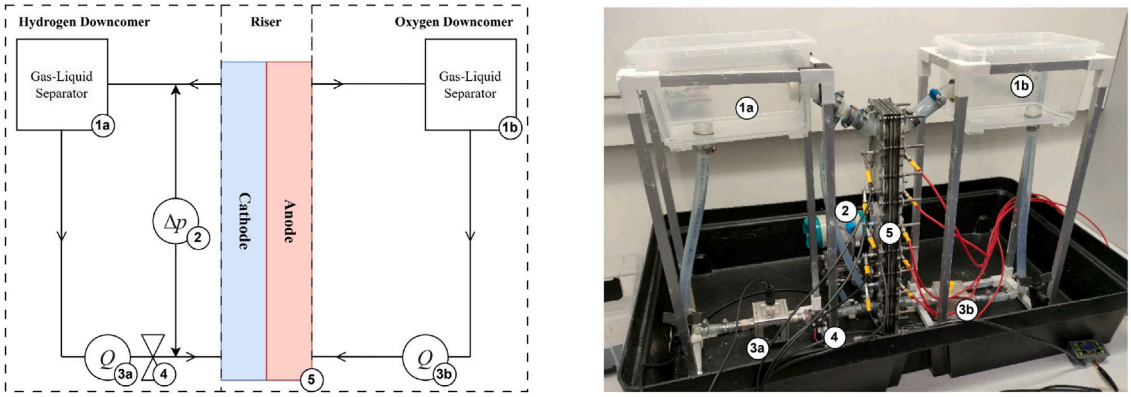

Fig. 4. Schematic diagram of the experimental setup on the left and an image of the experimental setup on the right. (1a) and (1b) are the gas–liquid separators for the cathode and anode side, respectively. (2) is the Siemens pressure transmitter. (3a) and (3b) are the Kobold flow meters. (4) is the Bürkert solenoid valve. (5) is the electrolysis stack, which contains the riser. An exploded view of the stack is shown in Fig. 5.

inertial contribution, Q_i, will be far more dominant than the laminar contribution to the pressure drop.

By inserting the second, riser, part into Eq. (4), we obtain the pressure drop of a planar Hagen–Poiseuille flow, valid for a fully-developed two-dimensional flow ($l_y \gg l$) between parallel plates,

$$\Delta p_{f,R} = 12\mu \frac{h}{l^2} W_l \tag{6}$$

Of course, the actual pressure drop will be substantially different due to the presence of gas bubbles, so this represents a significant simplification. We can take the important effect of gas bubbles into account by modifying the dynamic viscosity μ. An often-used relation for this increase is due to Krieger and Daugherty [34], which was developed for solid particles. It diverges for a volume fraction equal to ε_m that may be related, but in principle does not have to be the same as ε_{max}:

$$\mu = \mu_l f_v = \mu_l \left(1 - \frac{\varepsilon}{\varepsilon_m}\right)^{-2.5\varepsilon_m}. \tag{7}$$

This apparent viscosity, μ, will be greater than the liquid viscosity, μ_l, at elevated gas fractions. An overview of the models and experimental data on this viscosity increase can be found in Ref. [35]. Vogt [36] proposed a relation for the apparent viscosity for small bubbles in electrolytes and estimated a twofold rise in apparent viscosity at gas fractions of around 30%. Besides the viscosity increase, there is an extra length just before and just after the electrode, which slightly increases the laminar pressure drop. To keep the modelling relatively simple, we will instead use a constant correction factor f_v, which is unity for a flow that is predicted by single-phase Hagen–Poiseuille.

Due to the uncertainties and the lack of current knowledge on the pressure drop in electrolysers, it is recommended to use an empirical fit from pressure data, or to get a rough estimate for this correction factor using an apparent viscosity relation, such as given by the works of Krieger–Dougherty [34] or Vogt [36].

2.3. Analytical flow rate solution

Let us rewrite the average gas fraction of Eq. (2) in terms of flow rates

$$\langle \varepsilon \rangle = \frac{1}{2} \frac{Q_g}{Q_l + Q_s} \tag{8}$$

where

$$Q_s \equiv l l_y w_s + \frac{Q_g}{2\varepsilon_{max}} \tag{9}$$

is the upwards gas flow rate including slip [37]. Inserting Eqs. (3) and (8) into the pressure balance $\Delta p_f = \Delta p_H$ then gives

$$\frac{Q_l}{Q_v} + \left(\frac{Q_l}{Q_i}\right)^2 = \frac{Q_g}{Q_l + Q_s} \tag{10}$$

The solution to this cubic function for the recirculation flow rate, Q_l, is somewhat cumbersome due to lengthy expressions and the imaginary part of the roots. Instead, here we combine the limits of Eq. (10) to find the approximate solution:

$$Q_l \approx \frac{1}{\sqrt{\frac{Q_s^2}{Q_v^2 Q_g^2} + \frac{Q_s}{Q_i^2 Q_g} + \left(\frac{1}{Q_i^2 Q_g}\right)^{2/3} + \frac{1}{Q_v Q_g}}} \tag{11}$$

This solution gives a maximum relative error $\frac{Q_{l,numeric} - Q_{l,analytic}}{Q_{l,analytic}} = 13.4\%$ for values of Q_s, Q_v, Q_i and Q_g bounded between 10^{-12} and 1 m^3/s. An extended derivation of Eq. (11) can be found in Appendix B in the Supplementary Information.

Large electrolyser stacks will have larger electrolyte flow rates; therefore, Q_v and Q_i will also be larger. Compared to the limited width of the electrodes we used in our validation, scale-up can be easily achieved by increasing the electrode surface area by increasing the electrode width, l_y, which results in a higher product gas flow rate, Q_g. Creating a stack of multiple cells is equivalent to scaling l_y, as the flow behaviour is independent of the y-directions, with only the liquid and gas flow rates increasing.

The relatively simple Eq. (11) is highly useful for understanding the scaling in a natural recirculation electrolyser. It clearly shows the various limits, including $Q_l \approx \left(Q_i^2 Q_g\right)^{1/3}$ and $Q_l \approx \sqrt{Q_v Q_g}$ for low current densities and slip so that Q_s can be neglected. Eq. (11) generalises equation 6.C.35 of Ref. [24] to include viscous downcomer friction.

Inserting expressions gives *for negligible slip and low gas flux* ($Q_s \to 0$)

$$Q_l \approx \begin{cases} \left(Q_i^2 \frac{j\mathcal{V}_m}{nF} h l_y\right)^{1/3} & \left(Q_g^{1/3} \gg Q_i^{4/3}/Q_v\right) \\ \sqrt{\frac{\rho g l^3}{24\mu} \frac{j\mathcal{V}_m}{nF} h l_y^2} & \left(Q_g^{1/3} \ll Q_i^{4/3}/Q_v\right) \end{cases} \tag{12}$$

The former limit dependence on $j^{1/3}$ was found previously analytically in Ref. [23] and is included in Ref. [24]. The latter dependence on $j^{1/2}$ was found empirically in Ref. [38].

In the opposite limit of high gas flux, so that Q_s dominates Eq. (11) gives for dominant inertial friction $Q_l \approx Q_i \sqrt{Q_g/Q_s}$ and for dominant viscous friction $Q_l \approx Q_v Q_g / Q_s$. For negligible slip, $Q_g/Q_s \approx 2\varepsilon_{max}$, so that the dependence on gas flux disappears. Inserting expressions gives, for *negligible downcomer resistance and slip and high gas flux* ($Q_s \to \infty$)

$$Q_l \approx \begin{cases} \sqrt{2\varepsilon_{max}} Q_i & (Q_v \gg Q_i) \\ \varepsilon_{max} \frac{\rho g l^3 l_y}{12\mu} & (Q_v \ll Q_i) \end{cases} \tag{13}$$

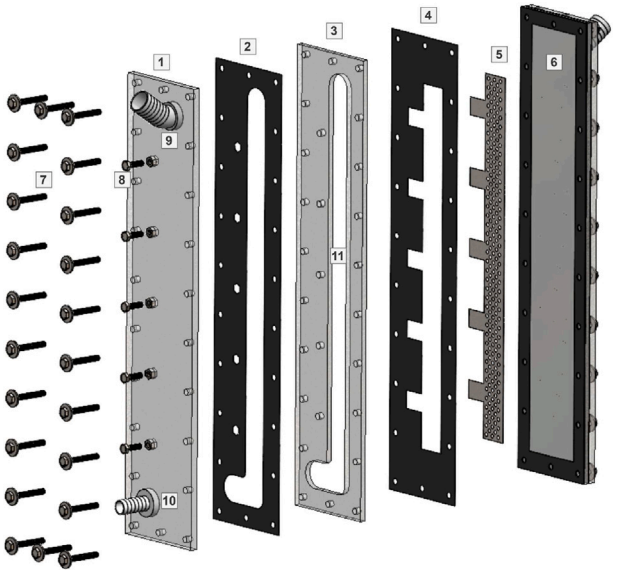

Fig. 5. Exploded view of the riser. (1) PMMA endplate containing the electrical connections (8), riser inlet (10) and outlet (9). (2,4) Rubber gaskets. (3) PMMA plate with the riser channel (11), the thickness of the plate can be changed to alter the electrode wall gap, l. (5) Expanded nickel electrode. (6) Zirfon UTP 500 diaphragm. (7) connection bolds.

These are simply the results from balancing inertial or viscous friction to buoyancy with a constant gas fraction ϵ_{max}. The former inertial limit can also be found in Ref. [24].

The power of Eq. (11) is that it combines all these known and new limits into a single easy-to-use expression that can be widely used for simple engineering estimates, including usually neglected effects like bubble slip, a maximum gas fraction, and both viscous and inertial pressure losses.

Note that when slip can be neglected, $Q_g/Q_s \approx 2\epsilon_{max}$, the liquid flow rate increases with increasing l until it becomes independent of l, for both low and high gas fluxes.

3. Experimental methods

To validate the introduced models in the preceding section, an in-house setup, shown in Fig. 4, was made. The setup consists of two parts, the riser and the downcomer, schematically shown on the left of Fig. 4.

It is essential to prevent the oxygen and hydrogen gases from mixing. Therefore, a diaphragm is placed between the anode and cathode, which creates a separate oxygen and hydrogen side. Both sides have their own riser channel, which is the space between the back wall and the electrode, shown in Fig. 3, and their downcomer. Each downcomer is equipped with a flow meter and a gas–liquid separator.

Fig. 5 shows an exploded view of the riser section. It consists of an electrolysis cell made from sandwiched PMMA plates and EPDM rubber gaskets. The electrodes are 0.5 mm thick expanded nickel and are positioned directly on top of a Zirfon UTP 500 membrane, which makes a zero-gap configuration. To supply current for the reaction, a Delta Elektronika SM 45–140 is connected to five stainless steel bolts which are pressed on the electrodes. The electrolyte used for the cell is 30 wt% KOH (6.9 M) at atmospheric conditions. The properties of KOH under these conditions can be found in Table 1. The electrode–wall gap, l, can be adjusted by stacking PMMA plates with varying thicknesses between the electrode and the end plate. All geometrical values can be found in Table 1.

At the top of the electrolysis cell, the flow exits into the downcomer through a 16 mm inner diameter PVC tube. After leaving the cell, the flow enters the gas–liquid separator, where the gaseous products are separated from the electrolyte stream. The electrolyte then recirculates down and passes through the Kobold MIM-1305H-G4-C3T flow meter with a 0.2 mL/s resolution, where the flow rate is measured for four minutes for each current density at a 4 Hz frequency. Next, the flow passes a Bürkert PSV 239079 solenoid valve, which is used to control the flow (always open in this study) and enters back into the bottom of the riser. A Siemens D-76181 Sitrans P Differential Pressure Transmitter measured the pressure drop over the cell. This transmitter is connected to the riser's inlet and outlet. The measured pressure drop is used to estimate the characteristic flow rate coefficients Q_v and Q_i in the results section.

Table 1
Properties of the setup.

Variable	Notation	Value
Electrode–wall distance	l	1–16 mm
Riser channel/electrode height	h	400 mm
Riser channel width	l_y	30 mm
Electrolyte concentration	c	6.9 M/30 wt%
Electrolyte density	ρ	1292 kg m^{-3} [39]
Electrolyte viscosity	μ_l	1.9 mPa s [40]
Maximum gas fraction	ϵ_{max}	0.71
Slip velocity (H_2)	w_S	14 mm s^{-1}
Slip velocity (O_2)	w_S	20 mm s^{-1}
Molar volume	$\mathcal{V}_m$	0.0224 m^3 mol^{-1}
Characteristic inertial flow rate	Q_i	27.5 mL s^{-1}
Characteristic viscous downcomer flow rate	$Q_{v,D}$	115.6 mL s^{-1}
Viscous correction factor (cathode)	f_v	3
Viscous correction factor (anode)	f_v	2.5
Inertial correction factor (cathode/anode)	f_i	1.5

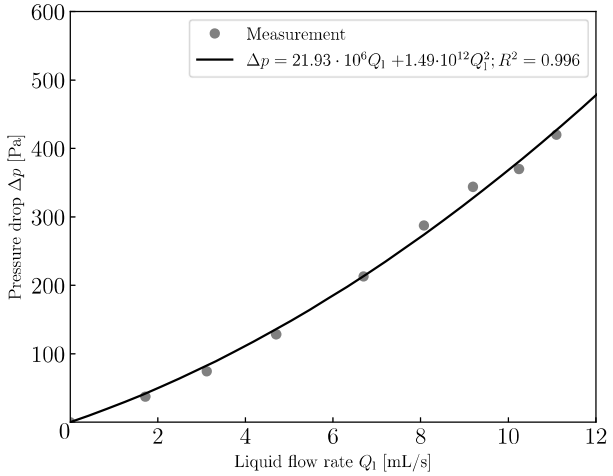

Fig. 6. Pressure drop across the downcomer with a regression based on Eq. (4). The riser gap was $l = 5.4$ mm.

4. Results

The models introduced in the theory section are here experimentally validated with our in-house setup. First, we fit the downcomer's characteristic viscous and inertial flow rate, $Q_{v,D}$ and Q_i, using the measured pressure drop.

Fig. 6 shows the pressure drop data points with a regression based on Eq. (4) to determine $Q_{v,D}$ and Q_i. The measurements for these characteristic flow rates were conducted with an electrode–wall gap of 5.4 mm since this gives a high flow rate, which allows pressure drop measurement over a wide range. The values were found to be: $Q_{v,D} \approx \frac{\frac{1}{2}\rho g h}{21.93 \cdot 10^6} \approx 115.6$ mL/s and $Q_i \approx \frac{1}{f_i}\sqrt{\frac{\frac{1}{2}\rho g h}{1.49 \cdot 10^{12}}} \approx \frac{41.25}{f_i}$ mL/s. Q_i,

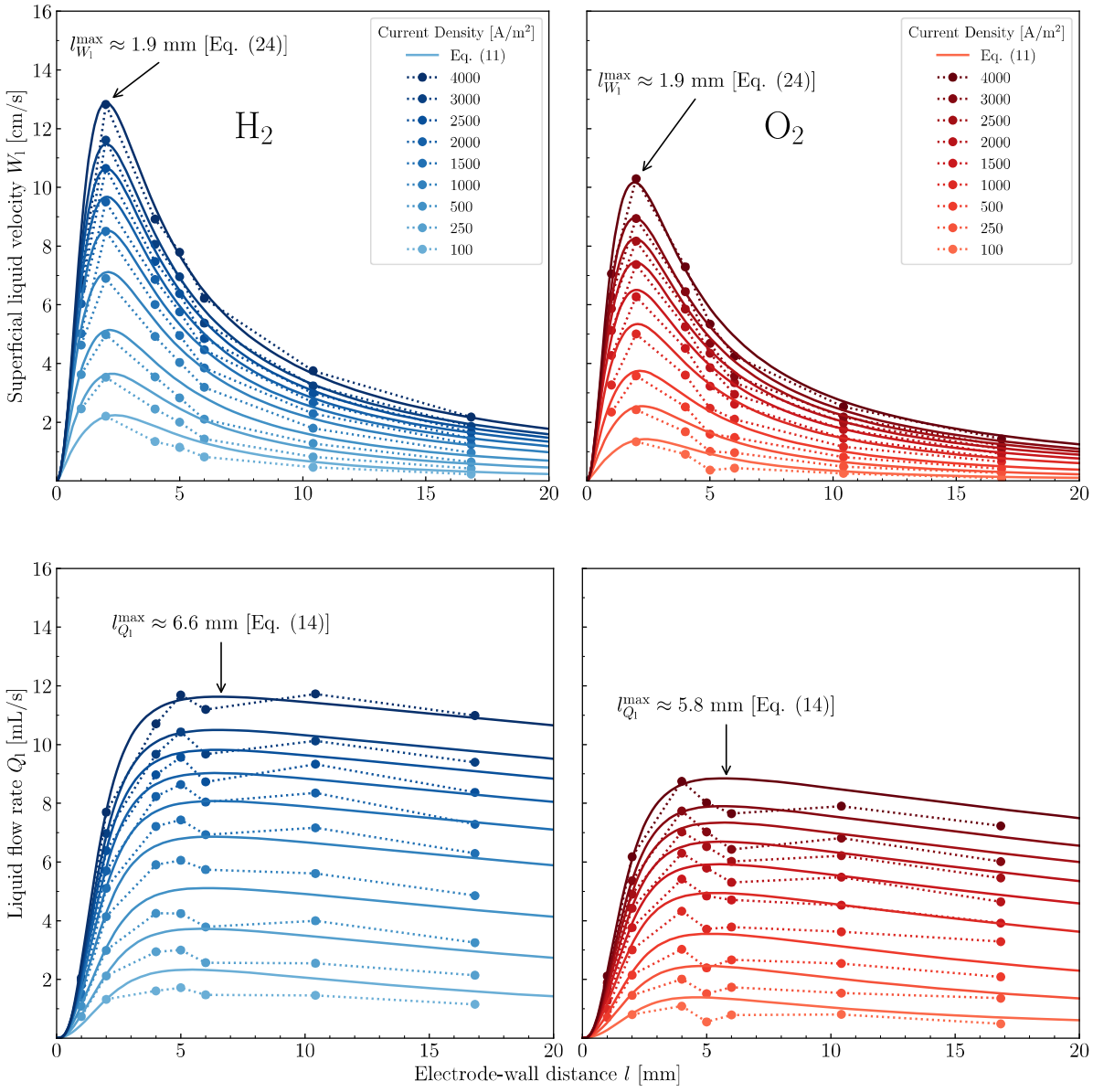

Fig. 7. Superficial liquid velocity W_l (top) and liquid flow rate Q_l (bottom) plotted as a function of electrode–wall distance for current densities ranging from 100 to 4000 A/m^2. The velocity is obtained by dividing the flow rate by the cross-sectional riser area, $l_y l$. The solid lines represent Eq. (11). The dots are experimental data from four-minute flow measurements with a 4 Hz measurement frequency. The flow rate was found to have a negligible variance during this time period. The connected dashed lines are to guide the eye. The solid lines are plotted using Eq. (11). The peaks of the four plots are indicated with the numerical value from Eqs. (24) for the velocity and (14) for the flow rate, which shows very good agreement between model and experimental data. For the hydrogen side, the slip velocity is set to 1.4 cm/s, $f_v = 3$ and $f_i = 1.5$, for the oxygen side, the slip velocity is set to 2 cm/s, $f_v = 2.5$ and $f_i = 1.5$.

here, is in the same order as from Ref. [22] which we estimate to be $Q_i \approx 15 - 300$ mL/s, depending on their downcomer size.

Note from the schematic on the left of Fig. 4 that our measurement excludes the inlet and outlet of the riser. Additionally, the flow in the riser is not fully developed because of the short length, which leads to an increased inertial pressure drop. To compensate for this, we divide the measured value by a correction factor, $f_i \approx 1.5$, increasing the inertial pressure drop.

Besides the inertial correction factor, the planar Poiseuille flow in the riser has to be corrected for the presence of bubbles, which causes a viscosity increase according to Eq. (7). These discrepancies will be overcome by the fitting factors f_v and f_i applied to Eq. (5) and Q_i, respectively.

Fig. 7 shows the measurements of the natural recirculation flow rate for various current densities. During the four-minute measurements, the flow was found to be stable with a negligible variance. In the same graph, the analytical solution for the flow rate, Eq. (11), is plotted. The flow rate increases with increasing electrode–wall distance, l, as the frictional riser pressure drop of Eq. (6) decreases. As l increases, the average gas fraction in the riser, $\langle\varepsilon\rangle$, which drives the flow, decreases. For large l, the riser frictional pressure drop becomes negligible compared to the downcomer pressure drop, which is independent of l. In this case, the average gas fraction also becomes independent of l because an increase leads to an inversely proportional decrease in liquid velocity. The only dependence on l is through the slip velocity in Eq. (9). As l increases, this slip contribution to the flow increases, leading to the decrease in flow rate shown in Fig. 7 (bottom). In addition to the flow rate, the figure contains a graph of the superficial liquid velocity, which peaks at an electrode–wall distance of around 2 mm. The average relative difference between the experimental and analytical model was found to be minimal for a viscous correction factor $f_v = 3$ for the cathode and $f_v = 2.5$ for the anode. The inertial correction factor was

found to be $f_i = 1.5$ for both. The correction factors reduce the average relative error between the model and the experimental data from 36% to 11% for the cathode and 29% to 7% for the anode. The 1.5 factor for inertial losses is most likely caused by the entrance and exit effect of the riser's inlet and outlet, which is not measured by the pressure drop meter. The large viscous correction factor could be due to the increased viscosity in the riser. For example, if we use Eq. (7), we find that an average gas fraction of 33% and 29% will give an increase in viscosity of 3 and 2.5, respectively. An additional contribution arises due to a small extra channel length before and after the electrode. Furthermore, we find that a slip velocity of 1.4 cm/s at the cathode side and 2 cm/s at the anode side captures the experimental data best, corresponding to a bubble size with an approximate diameter of 220 μm at the cathode and a 270 μm at the anode[1] [41]. This slip velocity addresses the decline in flow rate at large gaps and lower current densities. A direct estimate of the slip velocity can be obtained by measuring the bubble size distribution. Unfortunately, this was not possible due to the high gas fraction in the electrolyser.

5. Optimisation

One of the advantages of an explicit analytical solution, like Eq. (11), is that it can be used for optimisation. Depending on the application, different metrics may be important. For efficient heat removal, a high liquid flow rate may be desired. For a traditional gap electrolyser, one may want to minimise the ohmic drop. For mass-transfer-limited reactions, a high shear rate may be important to maximise mass transfer. Finally, to minimise electrolyser volume, it may be important to choose the smallest possible l that keeps the gas fraction below an acceptable level.

5.1. Maximal flow rate

Since the majority of heat will usually be transported out of a cell by advection, maximising the liquid flow rate also approximately maximises the heat transport and minimises how much the electrolyte temperature will rise from inlet to outlet. This is often a key design criterion.

Additionally, for negligible wall slip in Eq. (2) the average gas fraction $\langle\varepsilon\rangle$ in the riser decreases with increasing W_l/W_g, which scales with l/W_l proportional to the flow rate. Therefore, maximising the liquid flow rate also approximately minimises the average gas fraction in the cell, which can be beneficial for minimising bubble resistance and overpotentials, current homogeneity, and avoiding gas accumulation leading to hotspots.

As observed below Eq. (13), and as is clear from Eq. (16), the larger the l, the larger the flow rate up to a maximum Q_∞. This conclusion will be different when slip velocity is included. Often, the first term under the square root of Eq. (11) can be neglected. In this case, we can maximise the flow rate by taking the derivative with respect to l, setting this to zero, and solving, giving

$$l_{Q_l}^{\max} = \left(\frac{72\mu}{\rho g}\frac{Q_i^2}{l_y^2 w_s}\right)^{1/4} \tag{14}$$

For the values in Table 1 this gives a value $l_{Q_l}^{\max} \approx 6.6$ mm for hydrogen and $l_{Q_l}^{\max} \approx 5.8$ mm for oxygen. This is indeed exactly where the solid curves in Fig. 7, indicating the analytical flow rate expression of Eq. (11), reach their maxima. From experimental values in Fig. 7, we see a prominent peak in flow rate for an electrode–wall distance of 5 mm for hydrogen and 4 mm for oxygen, close to these predicted values.

[1] The slip velocities where calculated using the relation from Ref. [41] $w_S = \sqrt{4d\frac{(g\mu/\rho)^{1/3}}{3C_D}}$, where $C_D = \frac{432}{d_*^3}\left(1+0.022d_*^3\right)^{0.54} + 0.47\left[1-\exp\left(-0.15d_*^{0.45}\right)\right]$, and $d_* = \left(g\rho^2/\mu^2\right)^{1/3} d$. Here, d is the bubble diameter.

5.2. Minimal ohmic drop

Some electrolysers employ a traditional design, where bubbles are generated and rise between the two electrodes with a separator in the middle. In this case, the gas will be fully in the ion pathways, unlike the zero-gap setup used in the experiments of this research. As the gas fraction increases with height, its effect on the electrolyte conductivity will cause the local current density to decrease. Tobias [42] obtained an analytical expression for the vertical current distribution, neglecting bubble slip. Nagai et al. [43–45] found an optimal gap that maximises the current at a given cell potential. However, these models used $\varepsilon = W_g/W_l$, which only holds for low gas fractions. The more general Eq. (2) was, for a given liquid flow rate, shown to lead to no such optimum in Ref. [24]. This may be different in the case of a natural convection-driven system.

The fully coupled current-distribution problem will be too challenging to approach analytically. Instead, we will assume a constant current density and ask which gap l minimises the following approximation for the ohmic drop, neglecting the slip velocity

$$\frac{jl}{\kappa_m\left(1-\langle\varepsilon\rangle\right)^{3/2}} = \frac{jl}{\kappa_m}\left(\frac{1}{1-\frac{1}{2Q_l/Q_g+1/\varepsilon_{\max}}}\right)^{3/2} \tag{15}$$

Without slip, we can write Eq. (11) as

$$Q_l \approx \frac{Q_\infty}{\sqrt{\left(\frac{l_v}{l}\right)^6 + \frac{Q_\infty}{Q_c}\left(\frac{l_v}{l}\right)^3 + 1}} \tag{16}$$

, where

$$Q_c \equiv \frac{1}{1/\varepsilon_{\max}Q_{v,D} + 2\varepsilon_{\max}/Q_g} \tag{17}$$

which tends to the smallest of $\varepsilon_{\max}Q_{v,D}$ and $Q_g/2\varepsilon_{\max}$. Q_∞ is the liquid flow rate in the limit $w_S = 0$ and $l \to \infty$ so that $Q_s = Q_g/2\varepsilon_{\max}$ and Q_v is replaced by $Q_{v,D}$:

$$Q_\infty \equiv \frac{1}{\sqrt{\frac{1/(2\varepsilon_{\max})^2}{Q_{v,D}^2} + \frac{1/2\varepsilon_{\max}}{Q_i^2} + \left(\frac{1}{Q_i^2 Q_g}\right)^{2/3} + \frac{1}{Q_{v,D}Q_g}}} \tag{18}$$

We additionally introduced the following length scale

$$l_v = \left(\frac{12\mu Q_\infty}{\rho g \varepsilon_{\max} l_y}\right)^{1/3} \tag{19}$$

Inserting Eq. (16), we minimise Eq. (15) with respect to l for $\varepsilon_{\max} = 1$, neglecting viscous downcomer friction so that $Q_c \approx Q_g/2$. In this case, an excellent approximation to the exact numerical solution with a relative error less than 4% is

$$l_{opt} = l_v\left(\frac{7/2}{1+\frac{2}{7}\left(\frac{2Q_\infty}{Q_g}\right)^2}\right)^{1/6} \tag{20}$$

In case of relatively low gas flux $Q_g \ll Q_\infty$, this reduces to

$$l_{opt} \approx \left(\frac{21\mu Q_g}{\rho g \varepsilon_{\max} l_y}\right)^{1/3} \tag{21}$$

Due to multiple assumptions used, we find this simple result, showing a proportionality with the current density to the power 1/3. This result is identical to the optimum obtained by Thiele and Schleiff [19], except for the slightly different prefactor. For extremely high gas flux $Q_g \gg Q_\infty$ Eq. (20) tends to $l_{opt} \approx (7/2)^{1/6} l_v \approx 1.23 l_v$, which is Eq. (21) with Q_g replaced by $1.07Q_\infty$.

Using the values from Table 1, we find that for high gas fractions, the optimum will lie at $l_{opt} \approx 1.8$ mm. This value is only slightly smaller than the electrode–wall distance that maximises the superficial liquid velocity, seen in Fig. 7.

In reality, small electrode–wall distances may lead to a change in the flow regime to slug flow. This was observed by, for example, Hine and Murakami [17], where they found that gaps smaller than 5 mm resulted in a slug flow in their 89-cm tall setup. This was also recently shown by Zhang et al. [33] at the same 5 mm gap where slug flow appeared at low 25% gas fractions. Both experiments were conducted in classical setups, without a separator. In this case, it may be wise to choose an electrode–wall distance that prevents an excessively high gas fraction, which will be discussed in paragraph 5.5.

5.3. Maximising shear rate

In some electrolysers, it is desirable to maximise mass transport from the electrodes to the bulk [46]. For hydrogen bubbles in alkaline electrolytes, it has recently been shown that this transfer is primarily due to the convective transfer of the electrolyte. [47]. Under laminar flow conditions, the heat and mass transfer coefficients are proportional to the wall shear rate to the power of 1/3.

For a fully developed single-phase laminar flow between two parallel plates, the wall shear rate is[2]

$$\dot{\gamma} = \frac{6Q_\mathrm{l}}{l_y l^2} \tag{22}$$

If we assume that the bubbles disperse approximately homogeneously horizontally and the flow remains laminar, we may use Eq. (22) to approximate the shear rate.

Neglecting bubble slip, we can insert Eq. (16) and find the electrode–wall distance, l, for which the shear is maximised. This is done by equating the derivative of Eq. (22) with respect to l to zero and solving this for l

$$l_{\dot{\gamma}}^{\max} = l_\mathrm{v}\left(\frac{Q_\infty}{8Q_\mathrm{c}}\left(-1+\sqrt{32\left(\frac{Q_\mathrm{c}}{Q_\infty}\right)^2+1}\right)\right)^{1/3} \tag{23}$$

This means that for $Q_\infty \gg Q_\mathrm{c}$ the optimum electrode–wall distance for maximised shear at the wall approaches zero. Very large gas flux $Q_g \gg Q_\infty$ will make $\frac{Q_\mathrm{c}}{Q_\infty} \approx \frac{1}{2}\sqrt{1+2\varepsilon_{\max}\left(\frac{Q_{\mathrm{v,D}}}{Q_\mathrm{i}^2}\right)^2}$. This means that $l_{\dot{\gamma}}^{\max}$ is constant with gas flux in this limit. For the values in Table 1, this optimum electrode–wall distance will be approximately 1.5 mm.

5.4. Maximum velocity

As a compromise between a desire to maximise flow rate and wall shear, one may want to optimise for maximum electrolyte velocity. In case both the heat or mass transfer rate to the electrode, and the temperature or concentration difference between inlet and outlet are important, maximising the velocity may be a sensible strategy. Maximising the liquid velocity minimises the residence time of the liquid in the riser, which may have advantages, for example, in terms of multiphase flow handling by minimising coalescence.

Dividing Eq. (11) by l, taking the derivative with respect to l and solving for l gives the electrode–wall distance that maximises the liquid velocity as

$$l_{W_\mathrm{l}}^{\max} = l_\mathrm{v}\left(\frac{Q_\infty}{4Q_\mathrm{c}}\left(1+\sqrt{32\frac{Q_\mathrm{c}^2}{Q_\infty^2}+1}\right)\right)^{1/3} \tag{24}$$

This reduces to $2^{1/6}l_\mathrm{v} = 1.22l_\mathrm{v}$ in case $Q_\mathrm{c} \gg Q_\infty$ and $l_\mathrm{v}\left(\frac{Q_\infty}{2Q_\mathrm{c}}\right)^{1/3} = \left(\frac{6\mu Q_\infty^2}{\rho g l_y \varepsilon_{\max} Q_\mathrm{c}}\right)^{1/3}$ when $Q_\mathrm{c} \ll Q_\infty$. So contrary to Eq. (23), because of the plus sign in Eq. (14), we find that the optimum does not tend to zero in the latter limit.

As mentioned in the previous paragraph, $\frac{Q_\infty}{Q_\mathrm{c}}$ does not increase with large gas flux $Q_\mathrm{g} \gg Q_\infty$. This means that $l_{W_\mathrm{l}}^{\max}$ assumes a constant value of 1.9 mm, given the values in Table 1.

5.5. Maximum gas fraction

Large electrolysers are often dimensioned for their capacity for gas removal. At too high gas fractions, coalescence of bubbles can cause dry zones near the top of the electrodes that impose a safety risk. Therefore, we choose l based on a maximum allowed gas fraction at the top of the electrode at height $z = h$: $\varepsilon_\mathrm{h} < \varepsilon_{\max}$. Eq. (8) gives the average gas fraction, but an expression for the gas fraction at the top of the electrode, when neglecting bubble slip, reads, $\varepsilon = \frac{Q_\mathrm{g}}{Q_\mathrm{l}+Q_\mathrm{g}/\varepsilon_{\max}}$. This equation is Eq. (29) written in terms of flow rates. Equating this to ε_m gives $\frac{1-\varepsilon_\mathrm{h}/\varepsilon_{\max}}{\varepsilon_\mathrm{h}} = Q_\mathrm{l}/Q_\mathrm{g}$. Inserting Q_l of Eq. (16) and solving for l gives

$$l_{\varepsilon_\mathrm{h}} = l_\mathrm{v}\left(\frac{1+\sqrt{1+\frac{4Q_\mathrm{c}^2}{Q_\infty^2}\left(\frac{Q_\infty^2}{Q_\mathrm{g}^2}\left(\frac{\varepsilon_\mathrm{h}}{1-\frac{\varepsilon_\mathrm{h}}{\varepsilon_{\max}}}\right)^2-1\right)}}{\frac{2Q_\mathrm{c}}{Q_\infty}\left(\frac{Q_\infty^2}{Q_\mathrm{g}^2}\left(\frac{\varepsilon_\mathrm{h}}{1-\frac{\varepsilon_\mathrm{h}}{\varepsilon_{\max}}}\right)^2-1\right)}\right)^{1/3} \tag{25}$$

For $\varepsilon_{\max} = 1$ and negligible viscous downcomer friction, so $Q_\mathrm{c} = Q_\mathrm{g}/2$, Eq. (25) simplifies to

$$l_{\varepsilon_\mathrm{h}} = \left(\frac{12\mu Q_\mathrm{g}}{\rho g l_y}\frac{1+\sqrt{1+\left(\frac{\varepsilon_\mathrm{h}}{1-\varepsilon_\mathrm{h}}\right)^2-\frac{Q_\mathrm{g}^2}{Q_\infty^2}}}{\left(\frac{\varepsilon_\mathrm{h}}{1-\varepsilon_\mathrm{h}}\right)^2-\frac{Q_\mathrm{g}^2}{Q_\infty^2}}\right)^{1/3} \tag{26}$$

Note that there is a minimum ε_h for this expression to be real. This effectively means that not all desired maximum gas fractions are possible. As the gas flux Q_g increases, the top gas fraction unavoidably becomes larger, whatever the choice for l. This limit is found when $\left(\frac{\varepsilon_\mathrm{h}}{1-\varepsilon_\mathrm{h}}\right)^2$ approaches $\frac{Q_\mathrm{g}^2}{Q_\infty^2}$, and therefore the minimum ε_h is

$$\varepsilon_{\mathrm{h,lim}} = \frac{Q_\mathrm{g}^2}{Q_\mathrm{g}^2+Q_\infty^2} \tag{27}$$

Usually, $Q_\mathrm{g} \ll Q_\infty$ so that Eq. (26) is again a very similar expression as was obtained in minimising the ohmic drop, Eq. (20), and maximising the wall shear, Eq. (23).

6. Conclusion

We derived an explicit analytical model for the flow rate in a gas-evolving electrolyser operating with natural recirculation. This model enables the determination of the influence of current density, electrode–wall distance, various fluid properties, and the slip between the liquid and gas phases on the flow rate, shear rate, and average gas fraction in the riser.

The flow rate can be approximated using Eq. (11) and shows excellent agreement with the experimental measurements in Fig. 7. In fitting the model, we increased the liquid viscosity by a factor $f_\mathrm{v} = 2.5–3$ to account for the influence of bubbles. We augmented the inertial losses by 50% to account for the inlet and outlet of the riser. We estimated the bubble slip velocities to be $w_\mathrm{s} = 14–20$ mm/s.

Furthermore, we optimised the electrode–wall distance in the setup for maximum flow rate in Eq. (14), shear rate in Eq. (23) and velocity in Eq. (24). Additionally, we found an optimum that minimises the ohmic drop in Eq. (20) for classical setups with inward-facing electrodes. These optima are mostly very similar, with values for our set-up ranging from 1.5 to 1.9 mm. For maximising the flow rate, we find significantly

[2] taking the derivative of the laminar Hagen–Poiseuille profile $6W_l(x/l)(1-x/l)$ with respect to x at $x = 0$ gives $\dot{\gamma} = 6W_l/l$, or Eq. (22). Multiplying with μ gives the wall shear-stress, integrating this over the total wall area $2hl_y$, neglecting the side-walls, gives the shear force and subsequently dividing by the flow area, $l_y l$, gives the frictional pressure drop of Eq. (6).

larger optimal values between 5.8 and 6.6 mm, depending on the current density. Besides these optimisation equations, we provided a relation, Eq. (25), for the electrode–wall distance that gives a desired maximum gas fraction.

The proposed model is general enough to be applied to electrolysers of various scales and detailed designs. On the other hand, it is simple enough to allow analytical optimisation, resulting in various highly useful optimisation expressions. Therefore, it serves as a highly useful tool for improving water electrolysers that utilise natural recirculation.

CRediT authorship contribution statement

G.B. Deiters: Writing – original draft, Visualization, Supervision, Methodology, Formal analysis, Data curation, Conceptualization. **J.R. de Vries:** Methodology, Investigation. **J.W. Haverkort:** Writing – review & editing, Supervision, Methodology, Funding acquisition, Formal analysis, Conceptualization.

Declaration of competing interest

The authors declare that they have no known competing financial interests or personal relationships that could have appeared to influence the work reported in this paper.

Acknowledgements

This publication is part of the project “Hydrogen bubbles quantified” (Vidi grant with project number 19665), which is (partly) financed by the Dutch Research Council (NWO), The Netherlands.

Appendix A. Supplementary data

Supplementary material related to this article can be found online at https://doi.org/10.1016/j.ijhydene.2025.152053.

References

[1] Trinke P, Haug P, Brauns J, Bensmann B, Hanke-Rauschenbach R, Turek T. Hydrogen crossover in PEM and alkaline water electrolysis: mechanisms, direct comparison and mitigation strategies. J Electrochem Soc 2018;165(7):F502.
[2] Haverkort J, Rajaei H. Electro-osmotic flow and the limiting current in alkaline water electrolysis. J Power Sour Adv 2020;6:100034.
[3] Chisti M, Halard B, Moo-Young M. Liquid circulation in airlift reactors. Chem Eng Sci 1988;43(3):451–7.
[4] Young MA, Carbonell RG, Ollis DF. Airlift bioreactors: analysis of local two-phase hydrodynamics. AIChE J 1991;37(3):403–28.
[5] Saez AE, Marquez MA, Roberts GW, Carbonell RG. Hydrodynamic model for gas-lift reactors. AIChE J 1998;44(6):1413–23.
[6] Mudde RF, Van Den Akker HE. 2D and 3D simulations of an internal airlift loop reactor on the basis of a two-fluid model. Chem Eng Sci 2001;56(21–22):6351–8.
[7] Zhang L, Yue C, Kang J, Wang W, Liu G, Liu Y. Influence of separation chamber structure on the performance of the anode chamber of a chlor-alkali cell. J Electrochem Soc 2017;164(4):E29.
[8] Alberto P. Bipolar diaphragm cell with vertical flow channels. 2009, British Patent 2, 051, 131, Filed 1980.
[9] Borrione P, Ottaviani A. Natural high flow rate recirculation: A highlight on de nora technologies membrane electrolyzers. Mod Chlor-Alkali Technol: Vol 5 1992;93–104.
[10] Donna PA. The effect of brine level on the voltage of mercury-type chlor-alkali cells. J Electrochem Soc 1974;121(10):1286.
[11] Diéguez P, Ursúa A, Sanchis P, Sopena C, Guelbenzu E, Gandía L. Thermal performance of a commercial alkaline water electrolyzer: Experimental study and mathematical modeling. Int J Hydrog Energy 2008;33(24):7338–54.
[12] Agranat V, Zhubrin S, Maria A, Hinatsu J, Stemp M, Kawaji M. CFD modeling of gas-liquid flow and heat transfer in a high pressure water electrolysis system. In: Fluids engineering division summer meeting. Vol. 47500, 2006, p. 649–56.
[13] Stiesdal H, Schibsbye K. An electrolysis system. 2022.
[14] Hinatsu J, Stemp M. Electrolyser module. 2013, US Patent App. 13/757, 511.
[15] Abdelouahed L, Valentin G, Poncin S, Lapicque F. Current density distribution and gas volume fraction in the gap of lantern blade electrodes. Chem Eng Res Des 2014;92(3):559–70.
[16] Kuhn M, Kreysa G. Modelling of gas-evolving electrolysis cells. II. Investigation of the flow field around gas-evolving electrodes. J Appl Electrochem 1989;19(5):677–82.
[17] Hine F, Murakami K. Bubble effects on the solution IR drop in a vertical electrolyzer under free and forced convection. J Electrochem Soc 1980;127(2):292.
[18] Roušar I. Pumping effect due to gas evolution in flow-through electrolysers. J Appl Electrochem 1987;17:134–46.
[19] Thiele W, Schleiff M. Zur optimierung der geometrischen abmessungen vertikaler elektrolyseure mit gasentwickelnden elektroden. 1979.
[20] Schleiff M, Thiele W, Matschiner H. Modellierung und technische nutzung gasentwickelnder elektroden. I: Modellierung zwangsdurchstroemter, gasentwickelnder vertikaler elektrolyseure.. 1982.
[21] Schleiff M, Thiele W, Matschiner H. Modellierung und technische nutzung gasentwickelnder elektroden. II: Modellierung gasentwickelnder elektrolyseure mit freier kreislaufstroemung des elektrolyten.. 1982.
[22] Thiele W, Schleiff M, Matschiner H. Modellierung und technische nutzung gasentwickelnder elektroden. III: Moeglichkeiten und grenzen der technischen nutzung des durch die disperse gasphase erzielten auftriebs des elektrolyten.. 1982.
[23] Gol’dberg A. Calculation of gas lift in vertical membrane electrolyzing cells with an electrolyte circulation contour. Russ J Electrochem 2000;36(6):645–53.
[24] Haverkort J. Electrolysers, fuel cells and batteries: Analytical modelling. TU Delft OPEN Publishing; 2024, p. 168.
[25] Zuber N, Findlay J. Average volumetric concentration in two-phase flow systems. 1965.
[26] Hills J. The operation of a bubble column at high throughputs: I. Gas holdup measurements. Chem Eng J 1976;12(2):89–99.
[27] Clark N, Flemmer R. The effect of varying gas voidage distributions on average holdup in vertical bubble flow. Int J Multiph Flow 1986;12(2):299–302.
[28] Coenen E, Janssen L. Voidage of bulk solution in a tall vertical gasevolving cell. J Appl Electrochem 1997;27:1143–8.
[29] Sigrist L. Verfahrenstechnische aspekte von elektrolysezellen mit stark gasenden elektroden (Ph.D. thesis), (6286). ETH Zurich; 1978.
[30] Kreysa G, Kuhn M. Modelling of gas evolving electrolysis cells. I. The gas voidage problem. J Appl Electrochem 1985;15(4):517–26.
[31] Vogt H. The voidage problem in gas-electrolyte dispersions. J Appl Electrochem 1987;17(2):419–26.
[32] Kellermann H, Jüttner K, Kreysa G. Dynamic modelling of gas hold-up in different electrolyte systems. J Appl Electrochem 1998;28:311–9.
[33] Zhang H, Zhang R, Chen Z, Yuan F, Yang Q, Liu B. Experimental and theoretical study on the gas holdup feature in a 1.5-m tall alkaline water electrolytic cell. AIChE J 2025;71(6):e18814.
[34] Krieger IM, Dougherty TJ. A mechanism for non-Newtonian flow in suspensions of rigid spheres. Trans Soc Rheol 1959;3(1).
[35] Konijn B, Sanderink O, Kruyt NP. Experimental study of the viscosity of suspensions: Effect of solid fraction, particle size and suspending liquid. Powder Technol 2014;266:61–9.
[36] Vogt H. Proposed prediction method for the frictional pressure drop of bubble-filled electrolytes. J Appl Electrochem 1982;12(3):261–6.
[37] Nicklin D. Two-phase bubble flow. Chem Eng Sci 1962;17(9):693–702.
[38] Boissonneau P, Byrne P. An experimental investigation of bubble-induced free convection in a small electrochemical cell. J Appl Electrochem 2000;30:767–75.
[39] Gilliam R, Graydon J, Kirk D, Thorpe S. A review of specific conductivities of potassium hydroxide solutions for various concentrations and temperatures. Int J Hydrog Energy 2007;32(3):359–64.
[40] Kuznetsov KI, Skorodumov SV, Granchenko PP. Measurements of the dynamic viscosity and density of KOH solutions at atmospheric pressure. High Temp 2020;58(6):806–11.
[41] Cheng N-S. Comparison of formulas for drag coefficient and settling velocity of spherical particles. Powder Technol 2009;189(3):395–8.
[42] Tobias CW. Effect of gas evolution on current distribution and ohmic resistance in electrolyzers. J Electrochem Soc 1959;106(9):833.
[43] Nagai N, Takeuchi M, Nakao M. Effects of generated bubbles between electrodes on efficiency of alkaline water electrolysis. JSME Int J Ser B Fluids Therm Eng 2003;46(4):549–56.
[44] Nagai N, Takeuchi M, Kimura T, Oka T. Existence of optimum space between electrodes on hydrogen production by water electrolysis. Int J Hydrog Energy 2003;28(1):35–41.
[45] Nagai N, Takeuchi M, Nakao M. Influences of bubbles between electrodes onto efficiency of alkaline water electrolysis. Pac Cent Therm Fluids Eng 2003;10:F4008.
[46] Hiraoka S, Yamada I, Mori H, Sugimoto H, Hakushi N, Matsuura A, Nakamura H. Mass transfer and shear stress on a vertical electrode with gas evolution. Electrochim Acta 1986;31(3):349–54.
[47] Haverkort J. A general mass transfer equation for gas-evolving electrodes. Int J Hydrog Energy 2024;74:283–96.